Journal of Applied Polymer Science

Preparation of Transparent PMMA/$Fe(IO_3)_3$ Nanocomposite Films from Microemulsion Polymerization

Latifa Houf,[1] Yannick Mugnier,[1] Didier Rouxel,[2] Ronan Le Dantec,[1] Laurent Badie,[2] Brice Vincent,[2] Cécile Coustal,[3] Sandrine Beauquis,[1] Charlotte Thevenet,[3] Christine Galez[1]

[1]Université de Savoie, SYMME, BP 80439, 74944, Annecy Le Vieux, Cedex, France

[2]Département P2M-UMR CNRS n°7198, Institut Jean Lamour, Universite Henri Poincaré Nancy 1, BP 239, 54506, Vandoeuvre-les-Nancy, Cedex, France

[3]PLASTIPOLIS, Pôle de compétitivité Plasturgie, BP 10029 Bellignat, 180 rue Pierre et Marie Curie, 01115 Oyonnax, Cedex, France

Correspondence to: Y. Mugnier (E-mail: yannick.mugnier@univ-savoie.fr).

ABSTRACT: Polymethyl methacrylate (PMMA)/$Fe(IO_3)_3$ nanocomposite thin films are obtained by *in situ* particle generation in microemulsions and subsequent photopolymerization of a mixture containing methyl methacrylate, trimethylolpropane triacrylate, and crystallized iron iodate ($Fe(IO_3)_3$) nanorods. Hyper-Rayleigh scattering measurements combined with X-ray diffraction, transmission electron microscopy, and dynamic light scattering are first used to probe *in situ* the crystallization kinetics of iron iodate nanorods in water-in-oil microemulsions prepared with methyl methacrylate as the oil phase and marlophen NP12 as a surfactant. Trimethylolpropane triacrylate is then added as a crosslinker before spin-coating. Films are deposited on glass substrates for the nonlinear optical characterizations and on silicon wafers for the piezoelectric and mechanical measurements. Nanocomposite films treated by corona discharge are finally characterized through optical microscopy, *laser Doppler vibrometry*, and Brillouin spectroscopy.
 J. Appl. Polym. Sci. 130: 1203–1211, 2013

KEYWORDS: colloids; crystallization; nanoparticles; nanowires and nanocrystals; nanostructured polymers; dielectric properties

Received 27 December 2012; accepted 9 March 2013; Published online 19 April 2013
DOI: 10.1002/app.39271

INTRODUCTION

As an alternative to bulk materials, organic/inorganic polymers and clay-based nanocomposites can find promising applications in nonlinear optics[1–3] and in the field of piezoelectric sensors.[4–6] Synthesis and microstructuring of bulk crystals, for instance lithium niobate, indeed require expensive and delicate steps[7] so that the nanocomposite approach receives more and more attention due to the conformability, versatility, lower density, and easy shaping of the polymer matrix as well as the possibility to benefit from the intrinsic functional properties of its inorganic constituents.[8–11] However, as far as noncentrosymmetric fillers are concerned, the "tensorial nature" of piezoelectricity and nonlinear optics implies a homogeneous dispersion of the nanoparticles within the matrix together with a strict control of their individual orientation in order to obtain a significant contribution of the inorganic fillers.[12]

Because of its polar structure and facile synthesis from coprecipitation in aqueous solution, iron iodate is here chosen as a model material for the inorganic part.[13,14] The nonlinear optical properties of $Fe(IO_3)_3$ were already demonstrated from powder measurements[15] and also at the single nanocrystal scale in a series of proof-of-concept experiments[16–18] focused on the use of nanometer-sized acentric nanocrystals, also called "harmonic labels," as new nonresonant exogenous biomarkers for second harmonic generation (SHG) microscopy.[19] $Fe(IO_3)_3$ nanoparticles crystallize in the space group $P6_3$ so that piezoelectric properties are allowed by the crystal structure even though measurements are not yet available because of the difficulty of obtaining quantitative values on nanocrystals by piezoresponse force microscopy and of growing bulk single crystals.[20] On the other hand, the needle-like $Fe(IO_3)_3$ crystalline nanoparticles obtained so far by coprecipitation of $Fe(NO_3)_3{-}9H_2O$ and HIO_3 in various sodium *bis*(2-ethylhexyl) sulfosuccinate (AOT)/alkane/water ternary systems are good candidates to prepare transparent functional polymers with optimized piezoelectric response.[12] The growth mechanism from water-in-oil microemulsions, clearly associated to an aggregation-induced crystallization of 10–20 nm amorphous precursor particles, leads to the formation of small crystalline nanorods with diameter and

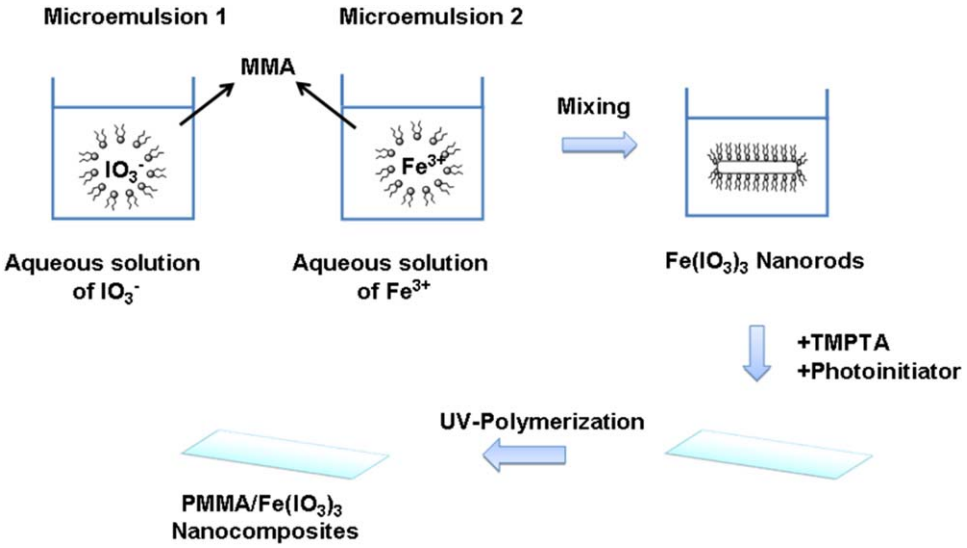

Figure 1. Preparation of PMMA/$Fe(IO_3)_3$ polymer nanocomposite thin films from the *in situ* particle generation approach. [Color figure can be viewed in the online issue, which is available at wileyonlinelibrary.com.]

length below 30 and 200 nm, respectively.[21] The nanometer size and the absence of aggregation are strong requirements in order to keep the transparency of the resulting nanocomposite material.[8]

In terms of preparation methods, polymer nanocomposites are always obtained after a primary dispersion of nanoparticles in a liquid, which can be a polymer melt, a polymer solvent or a monomer.[8] If dry powders are used as starting materials, powerful sonication treatments[22] are helpful to reduce the size of primary agglomerates. However, residual aggregates can limit the optical transparency, deteriorate the homogenized mechanical properties and here, prevent a unique particle orientation. Additionally, phase separation and sedimentation are commonly observed with inorganic nanoparticles that often tend to agglomerate. Two strategies were thus developed to preserve a homogeneous dispersion, namely the "*in-situ* polymerization" and the "*in-situ* particle generation" approaches.[8,11] In the former case, particles are dispersed in a monomer solvent after surface modification by using grafting techniques or by adsorption of amphiphilic molecules or polymerizable surfactants. For the latter, if inorganic nanocrystals can be synthesized by a coprecipitation reaction in water, polymerization of reverse w/o monomer microemulsions is very convenient due to the templating-effect associated with the reaction medium and to the availability of various surfactants. This technique was already successfully applied by Henle and Kaskel for the preparation of transparent photochromic nanocomposites based on BiOX (X = Cl, I)[10] and by Althues et al. for luminescent YVO_4:Eu/polymer nanocomposites.[9] A similar route is used in this work combined with a corona discharge treatment to promote the orientation of the polar $Fe(IO_3)_3$ nanofillers. After photopolymerization, the polymer matrix consists in polymethyl methacrylate (PMMA), a well-known transparent thermoplastic polymer for which the incorporation of inorganic (centrosymmetric) fillers like SiO_2 was already described.[23,24] Similarly, the homogeneous dispersion of inorganic acentric fillers such as ZnO nanocrystals appears very pertinent for the development of transparent PMMA nanocomposites for UV-shielding applications.[25,26] However, implementation of a stable, long-lasting noncentrosymmetry in a polymer matrix like PMMA is still a challenge. To our knowledge, only two recent interesting attempts can be mentioned concerning the incorporation of $KTiOPO_4$ nanocrystals[27] and of DAST chromophores[28] in PMMA.

EXPERIMENTAL

Chemicals

Iron nitrate nonahydrate ($Fe(NO_3)_3.9H_2O$, ≥99.99%) and iodic acid (HIO_3, ≥99.5%) as reactants, AOT (sodium *bis*(2-ethylhexyl) sulfosuccinate, $C_{20}H_{37}NaO_7S$ ≥99%) as a surfactant, Trimethylol propanetriacrylate (TMPTA) as a crosslinker and methyl methacrylate (MMA) as a monomer were purchased from Sigma-Aldrich (France). Marlophen NP12 (ethoxylated NonylPhenyl ether with 12 EO units in average) as a nonionic surfactant and phenyl *bis*(2,4,6-triméthylzol) phosphine (Irgacure® 819) as a photoinitiator were provided free of charge by SASOL and BASF (France), respectively. All chemicals were used without further purification.

Synthesis and Characterization of $Fe(IO_3)_3$ Nanorods

The overall preparation method illustrated in Figure 1 starts with the preparation of two separate w/o microemulsions containing MMA as the oil phase and either iodic acid or iron nitrate dissolved in the aqueous phase. Droplet size before and after mixing of the two w/o microemulsions is estimated by Dynamic Light Scattering (Zetasizer Nano-ZS, Malvern Instruments). In addition, pseudo-ternary phase diagrams (as detailed in "Result and Discussion" section) were investigated by adding pure water or aqueous solutions of iodic acid or iron nitrate to mixtures of MMA/AOT or MMA/NP12. The domains of existence of microemulsions being identified, *in situ* crystallization

Table I. Composition and Phase Behavior in the MMA/AOT (0.5*M*) System with Aqueous Solutions of Iodic Acid, Iron Nitrate and After Mixing of the Two Mixtures at 23°C

Samples	*W*	$[IO_3^-]$ (*M*)	No. of phases with IO_3^-	$[Fe_3^+]$ (*M*)	No. of phases with Fe_3^+	No. of phases after mixing
A1	10	6	2 φ	2	2 φ	2 φ
A2	40	6	2 φ	2	2 φ	2 φ
B1	10	3	2 φ	1	2 φ	2 φ
B2	40	3	2 φ	1	2 φ	2 φ
C1	10	1	2 φ	0.33	1 φ	2 φ
C2	40	1	2 φ	0.33	2 φ	2 φ
D1	10	0.3	1 φ	0.1	1 φ	1 φ
D2	40	0.3	2 φ	0.1	2 φ	2 φ

Single phase (1φ) regions only exist for low reactant concentrations.

of iron iodate nanorods in microemulsions is then probed by time-dependent hyper-rayleigh scattering (HRS) measurements. The experimental setup was already detailed in a previous work.[21] After centrifugation (Sigma 2–16 centrifuge) of the reaction medium, the crystalline structure of nanorods is confirmed by X-Ray Diffraction (XRD) with Co-Kα (INEL CPS 120 with a position sensitive detector). The size and morphology of $Fe(IO_3)_3$ nanorods are finally investigated by transmission electron microscopy (Philips CN200) after dispersion in ethanol and drying of a drop in ambient conditions on a carbon-film-coated copper grid.

Preparation and Characterization of Nanocomposite Films

After coprecipitation between reactants and formation of crystallized nanoparticles, TMPTA (30.6 wt %), as a crosslinker to improve the mechanical properties of the PMMA/$Fe(IO_3)_3$ nanocomposites,[29] and the photoinitiator (3.4 wt % Irgacure® 819) are added to the MMA microemulsion (the % refers to the MMA weight content). The mixture is then spin-coated on standard microscope slides or on silicon wafers. In addition, as piezoelectric and nonlinear optical properties of the nanocomposite films strongly depend on the individual particle orientation, a *corona discharge treatment* (10 kV at 7 mm from the film surface and for 40 min at 75°C) *is applied* before the polymerization step. The radical photopolymerization of the monomer is then performed by UV irradiation (DP40, 12*15W, C.I.F.) for 30 min. Note also that the chemical structure of the resulting nanocomposites were not specifically investigated in this study because similar drying and UV irradiation conditions are already known to yield well-polymerized samples.[9,30,31]

Optical and piezoelectric properties of PMMA/$Fe(IO_3)_3$ nanocomposite thin films, treated or not by corona discharge, are investigated as follows. Detection of a nonlinear optical response is performed using the Maker-fringes technique. The experimental setup is the same as the one used for HRS[21] except that the signal at 2ω is detected in transmission (and not perpendicularly to the incident laser beam) and that the sample is placed on a rotation plate. Piezoelectric performances of the different films are assessed with a *piezo-d meter* (SS01-01, *Sensor Technology limited, Canada*) to estimate the d_{33} piezoelectric coefficient and also with *laser vibrometry* (SIOS *SP-S 120, Polytec*). *Sputtered-gold electrodes* are *first deposited* and amplitudes of the mechanical vibrations are measured versus the applied voltage. Finally, mechanical properties of nanocomposite films are characterized by Brillouin spectroscopy. The elastic constants c_{11} (longitudinal modulus) and c_{44} (shear modulus) are determined from the acoustic phonons frequencies measured within the films with an accuracy of $\pm$0.2 GHz.

RESULTS AND DISCUSSION

Large amounts of reactants, and subsequently of dispersed nanoparticles, are needed to obtain a significant response in terms of SHG properties and piezoelectricity.[12,23] Pseudo-ternary phase diagrams are thus first studied in the following with MMA as the oil phase and either with AOT as an anionic surfactant or with Marlophen NP12 as a nonionic one to find out the optimum experimental synthesis conditions.

Ternary Phase Diagrams with MMA as the Oil Phase

In regard to AOT, stability regions in the MMA/AOT/water ternary system were already identified at room temperature by the group of Kaskel and coworkers.[23] Following this work, iodic acid and iron nitrate were dissolved in water and their effects on the existence of reverse microemulsions were studied. The concentration of AOT was fixed at 0.5*M* and we then adjusted the concentration of iodic acid and iron nitrate, in stoichiometric amounts, from 6 to 0.3*M* and from 2 to 0.1*M*, respectively.

As shown in Table I, the ternary system containing MMA and AOT does not stabilize large amounts of water. The microemulsion phase boundary is even reduced in the presence of aqueous reactants[31] with the consequence that the yield of nanorods is small. In addition, a low concentration of reactants results in very slow crystallization kinetics. Typically, for sample D1 (see Table I), the apparition of $Fe(IO_3)_3$ crystalline nanorods is not detected through HRS measurements before 60 h, even at temperature above 50°C. Besides, after such a period, the viscosity is high and prevents any spin-coating. We demonstrated earlier that an increase in temperature and in the concentration of reactants and surfactants strongly reduces the crystallization time but such variations are not conceivable here.[21] Another possibility is to reduce the strong binding interactions at the organic–inorganic interface between surfactants and the surface of primary amorphous precursors.[32] AOT is thus replaced by Marlophen NP12 because nonionic surfactants quicken the overall crystallization mechanism and also allow higher water contents as illustrated in Figure 2 for the MMA/NP12/pure water ternary system. Single phase regions, transparent to the eye, can be detected after a few minutes of stirring at 23°C. It is also observed that the presence of a single phase is strongly temperature-dependent as already mentioned.[23,31]

In Figure 3, red and blue points indicate a single phase from the initial MMA/NP12 mixtures containing 60, 75, and 80 wt % of MMA, respectively. It shows that, after dissolution of iron nitrate (1*M*) and iodic acid (3*M*) at 23°C in the aqueous phase, the amount of stabilized water is reduced in the presence of

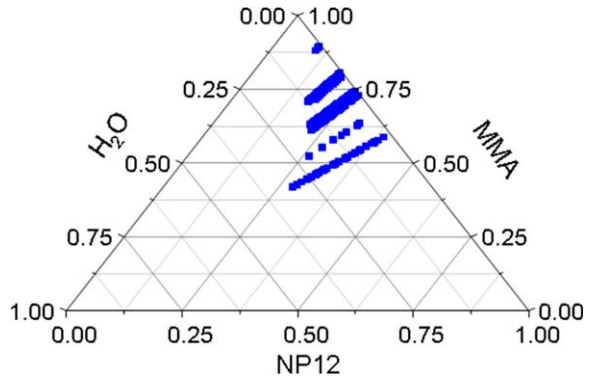

Figure 2. Partial phase diagram at 23°C of the water/MMA/ NP12 system. [Color figure can be viewed in the online issue, which is available at wileyonlinelibrary.com.]

Fe^{3+} ions. On the contrary, a relatively high concentration of aqueous iodic acid (3*M*) has almost no influence and a single phase region is still obtained for large amounts of water and, more generally, at high iodic acid concentrations when compared with AOT.

Growth Mechanism of $Fe(IO_3)_3$ Nanorods with MMA as the Oil Phase

Growth mechanisms of iron iodate nanocrystals are studied at 23°C from two mixtures of initial composition given in Table II. In both cases, a "milky" solution appears immediately after mixing of the initial w/o microemulsions of iodic acid (3*M*) and iron nitrate (1*M*). The formation of amorphous particles as evidenced by XRD (data not shown) and the fact that no HRS signal is detected, is probably related to a very fast nucleation caused by the absence of a single phase (i.e., a microemulsion) in the reaction medium (see Figure 4).

The lack of transparency precludes any optical applications based on crystallized noncentrosymmetric fillers. However, we observe that the addition in excess of an aqueous solution of IO_3^- (3*M*) allows one to obtain a microemulsion as shown in Figure 4. 10 and 3.5 wt % are thus necessary to recover the transparency of sample 1 and sample 2, respectively. In the resulting yellowish transparent reaction medium, distribution by number of DLS spectra indicates a mean size about 5–6 nm again in agreement with a single phase.

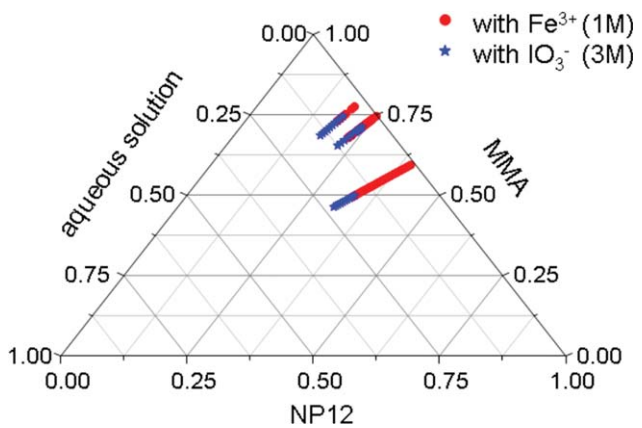

Figure 3. Partial phase diagram for MMA/Marlophen NP12/aqueous solution of IO_3^- (3*M*) and Fe^{3+} (1*M*). [Color figure can be viewed in the online issue, which is available at wileyonlinelibrary.com.]

Once a microemulsion is obtained, the real-time crystallization and formation dynamics of $Fe(IO_3)_3$ nanorods in the MMA/NP12/water ternary system are probed *in situ* by time-dependent HRS measurements as shown in Figure 5. Detection of a rapidly growing HRS signal can be attributed to the formation of the first crystallites whereas the quasi-linear increase accounts for the higher number of crystallized nanorods as well as their rise in size.[21] Interestingly, it can be noticed that the crystallization kinetics is much faster with MMA and NP12 than with alkane and AOT. In addition, the time-dependent HRS response reported in Figure 5 is comparable with the ones obtained with AOT[21] suggesting that a similar growth mechanism, namely an aggregation-induced crystallization,[33] accounts for the formation of iron iodate nanorods from primary amorphous precursors stabilized by surfactant molecules.

Such a growth mechanism is indeed confirmed by TEM observations as shown in Figure 6 where nanorods can be observed once a plateau is reached in the time-dependent HRS measurement. The corresponding X-ray diffraction profile (Figure 7) is found in good agreement with the structure of iron iodate refined from a coprecipitation powder in a surfactant-free aqueous solution.[13] Remarkably, the absence of significant shift between the experimental and calculated spectra indicates low binding interactions between primary particles and the surfactant layer as thoroughly discussed in Ref. 32. Fast rearrangements within organic–inorganic aggregates of amorphous particles stabilized by NP12 molecules are thus expected. This is indeed in agreement with the overall fast crystallization kinetics depicted in Figure 5.

Film Characterizations

The nanocomposite films are prepared according to the general protocol described in Figure 1 for two series of samples (with high and low initial water content) whose microemulsion compositions in weight percent, are reported in Table III. The samples differ in the initial reactant concentrations dissolved in stoichiometric amounts in the aqueous phase and the calculated content of iron iodate is indicated in the last column according to the initial water content. Assuming that all the produced nanorods have a mean diameter and length of 20 and 300 nm, respectively, this results to a final density number of nanorods that can be estimated at about 10^{13} per gram of nanocomposite.

After the initial mixing and the detection of a nonzero HRS signal attributed to the presence of crystallized nanorods, films were spin-coated either from the translucent solutions or from the "milky" solutions as shown in Figure 5. In the first case,

Table II. Composition (wt %) of the MMA/NP12/Aqueous Reactants Ternary System

Sample	MMA (%)	NP12 (%)	Aqueous solution (%)
1	50	33	17
2	75	18	7

Figure 4. Visual inspections of the two initial microemulsions, after their mixing and with an excess of iodic acid for sample 1 of Table II. [Color figure can be viewed in the online issue, which is available at wileyonlinelibrary.com.]

films are translucent and appear homogeneous in dark-field optical microscopy. Conversely, for films obtained from "milky" samples, nanorods at the end the crystallization process tend to sediment more quickly because of their size and of the presence of agglomerates. After deposition by spin-coating, optical inspections of films reveal a microstructure inconsistent with any further characterization.

SHG Properties

Starting from translucent solutions, the microstructure and homogeneity of spin-coated films on glass substrates were acceptable after corona orientation treatment and photopolymerization, as it can be seen by dark-field optical microscopy. A representative image is given in Figure 8 where iron iodate nanorods with random orientations are readily distinguishable at the film surface. Corona discharge treatments applied before the polymerization step are thus not fully efficient to promote a unique long-term nanorod orientation perpendicular to the film substrate.

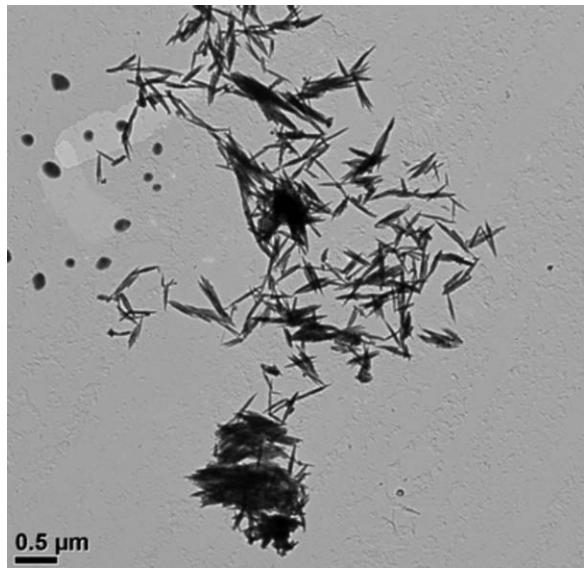

Figure 6. Typical TEM micrograph of sample 2 after centrifugation of the reactive medium at the end of the crystallization process.

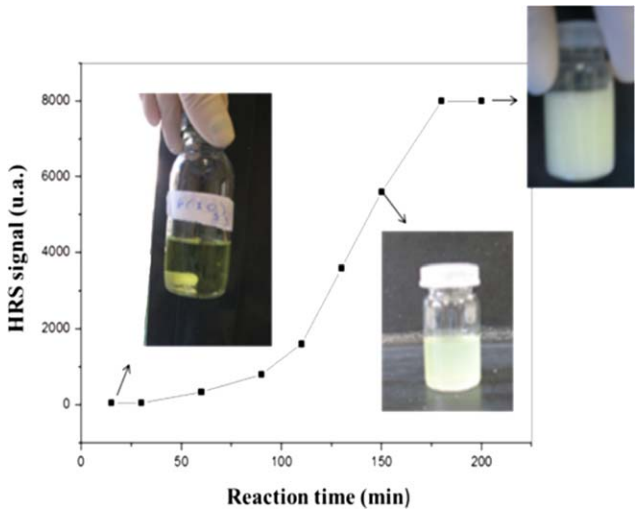

Figure 5. Time evolution of the HRS signal collected from sample 1 after addition of an excess of iodic acid. Each point corresponds to a 4 mL sample taken from the reaction medium maintained at 23°C. [Color figure can be viewed in the online issue, which is available at wileyonlinelibrary.com.]

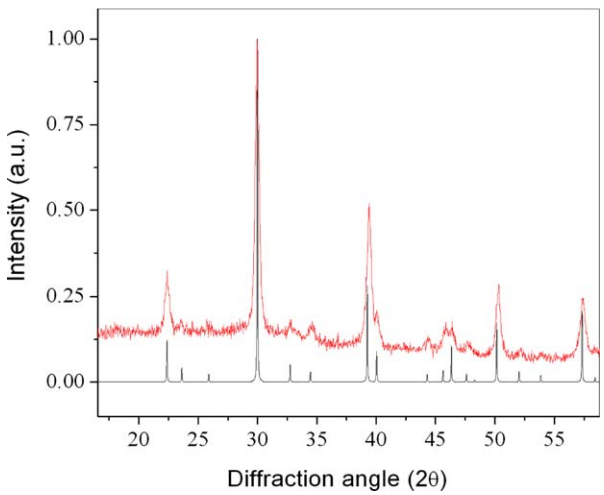

Figure 7. Comparison of the X-ray diffraction profile (Co and Kα) of sample 2 with the calculated one (ICSD #154674).[13] [Color figure can be viewed in the online issue, which is available at wileyonlinelibrary.com.]

Table III. Initial Microemulsion Composition and Theoretical $Fe(IO_3)_3$ Contents Presented in Weight Percent

Sample	$[Fe^{3+}]$ (M)	MMA	NP12	Irgacure	TMPTA	Water	$Fe(IO_3)_3$
A	1.0	35.9	23.9	1.8	16.6	18.2	3.5
B	0.7	36.3	24.2	1.9	16.8	18.4	2.5
C	0.4	36.6	24.4	1.9	17.0	18.6	1.4
D	1.0	52.2	12.5	2.7	24.2	7.1	1.4
E	0.7	52.4	12.5	2.7	24.3	7.2	1.0
F	0.4	52.6	12.6	2.7	24.4	7.2	0.6

The absence of electric field-induced orientation for spin-coated films on glass substrates is also evidenced with the Maker-fringes technique. A constant SH signal is indeed recorded in Figure 9 for an incident angle varying between −40° and +40°. The decrease on both sides originates from higher Fresnel coefficients. This optically incoherent SHG response can however, be attributed to the presence of iron iodate nanorods. At perpendicular incidence, a qualitative linear increase (data not shown) is observed from sample F to D and then from sample C to A in agreement with a higher content of nonlinear scattering particles.[34,35] For each sample, it is also noticed that the SH intensity increases with a quadratic dependence on the input laser power, as expected.

Mechanical Characterizations

Most potential applications for these nanocomposites, in piezoelectric devices as well as in nonlinear optics, require films with a sufficient mechanical strength. This mechanical behavior can be expressed in terms of tensile strength or wear resistance of the polymer film. Several studies have shown that the presence of nanoparticles could greatly enhance the adhesion of a polymer film by reducing its wear[24] or by reducing the formation and propagation of cracks. In this study, Brillouin spectroscopy is used to check that films retain a reasonable mechanical stiffness in spite of the eventual inclusions of water within the polymer matrix after the polymerization step. This technique, particularly attractive for the determination of elastic properties in solids and liquids, was successfully applied to transparent crystals and oligomers.[36,37] Other works also report that the sensitivity of Brillouin spectroscopy is also well suited for thin (thickness in the micrometer range) polymer nanocomposite films.[24,38,39] Here, because a highly reflecting substrate is required, PMMA/$Fe(IO_3)_3$ nanocomposite films are deposited on silicon wafers. The influence of TMPTA, water and iron iodate nanorods is studied separately.

Addition of the curing agent TMPTA leads to PMMA/PTMPTA copolymers showing, as expected, a net increase in the elastic constant c_{11} (longitudinal modulus) compared to PMMA alone (Figure 10, samples denoted as 1, 2, and 3). For the PTMPTA/PMMA samples, the increase attains 40–50% for c_{11} and a similar trend is observed for the c_{44} coefficient (shear modulus). Concerning the PMMA/NP12/PTMPTA/$Fe(IO_3)_3$ nanocomposite films (sample B and E of Table III), a main result is that

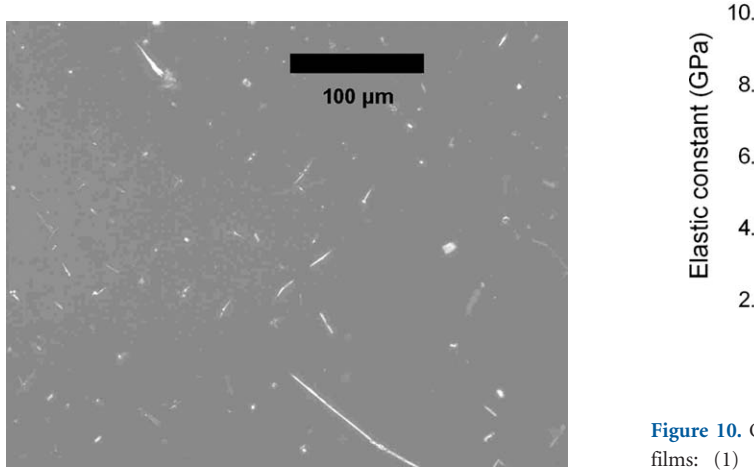

Figure 8. Representative dark-field image of a spin-coated PMMA/$Fe(IO_3)_3$ film on a glass substrate after corona discharge and polymerization.

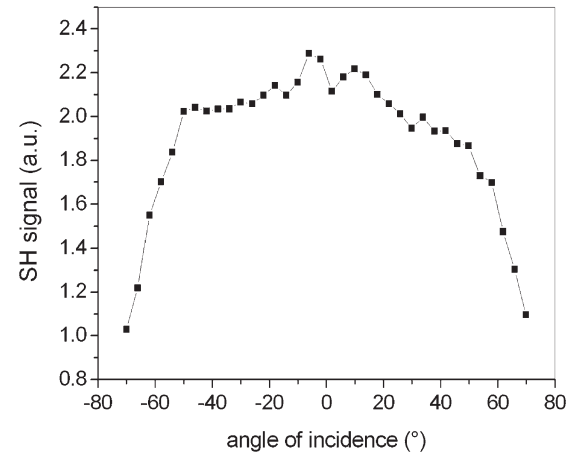

Figure 9. Typical transmitted SH signal according to the laser incident angle from the Maker-fringes setup.

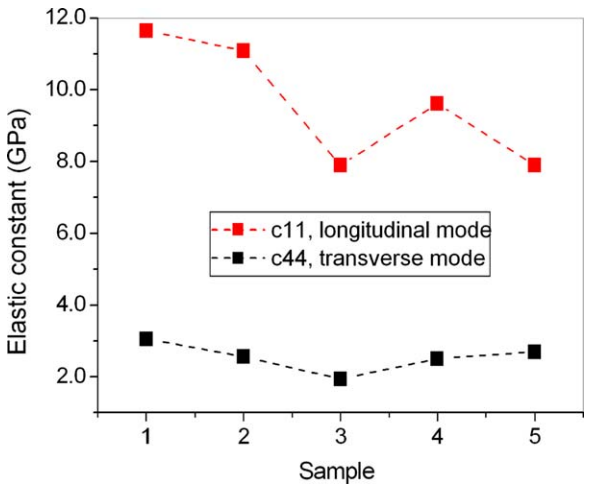

Figure 10. Comparison of the longitudinal and shear moduli for different films: (1) PMMA/PTMPTA (18%), (2) PMMA/PTMPTA (15%), (3) PMMA, (4) sample E, and (5) sample B of Table III. Dash line is a guide to the eye. [Color figure can be viewed in the online issue, which is available at wileyonlinelibrary.com.]

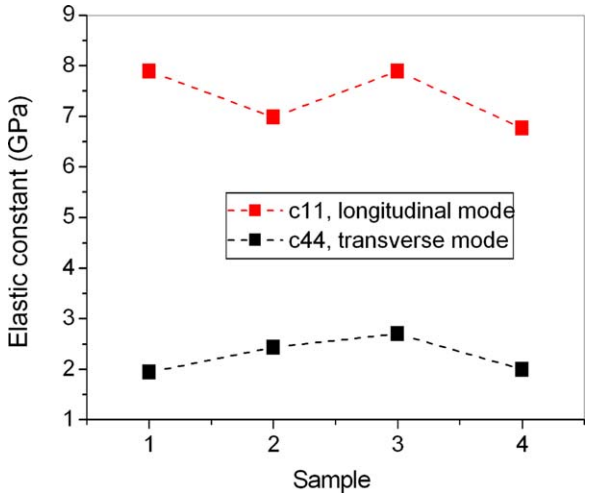

Figure 11. Comparison of the longitudinal and shear moduli for different films: (1) PMMA, (2) sample C, (3) sample B, and (4) sample A of Table III. Dash line is a guide to the eye. [Color figure can be viewed in the online issue, which is available at wileyonlinelibrary.com.]

the annealing temperature of 75°C applied during the poling step seems efficient to reduce the initial water content associated to the microemulsion process. The resulting mechanical properties are thus not significantly reduced comparatively to PMMA/PTMTA copolymers. On the contrary, a reinforcement of 7% is measured for sample E (sample 4 in Figure 10) in relation to pure PMMA. Interestingly, for a higher initial water and surfactant content, the elastic constant c_{11} for sample B (sample 5 in Figure 10), is similar to that of PMMA because of the compensating effect of PTMPTA.

Mechanical properties of films with various concentrations in iron iodate nanorods, obtained from initial microemulsions (~18 wt % water) with 0.4, 0.7, and 1*M* of Fe^{3+} in the aqueous droplets, are compared with pure PMMA in Figure 11. In this case, in spite of the different contents of inorganic fillers, no significant variation of the c_{11} and c_{44} elastic constants coefficients can be observed for the nanocomposites. This is probably due to the presence of NP12 molecules at the organic–inorganic interface between PMMA and $Fe(IO_3)_3$. Surfactants could thus prevent any reinforcement of the composite by the inorganic nanorods.

Piezoelectric Characterizations

In the literature, enhancement of the mechanical or dielectric properties of traditional piezoelectric polymers like P(VDF-TrFE) by inorganic nanofillers was already investigated.[38] Here a transparent nonpiezoelectric polymer, namely PMMA, is voluntarily selected to examine if electroactive nanofillers can induce a measurable piezoelectric response. A recent modeling study indicates that the d_{33} homogenized piezoelectric coefficient of a nanocomposite is expected to be low, typically in the $pC.N^{-1}$ range.[12] Accordingly, no piezoelectric response could be detected with the piezo-d-meter in the Berlincourt configuration.

Laser doppler vibrometry, based on interferometry, is thus used thereafter as a more sensitive technique. Originally developed by Zhang et al. at Penn State University for the study of piezoelectric and electrostrictive strains,[40] it was later shown that laser doppler vibrometry could also be used for evaluating the piezoelectric coefficient of thin films. This approach remains however technically tricky in the case of piezoelectric films because they undergo dimensional changes in three directions. Vibrations are expected to increase linearly in the direction of the applied electric field but the d_{31} and d_{32} coefficients may induce bending of the substrate.[41] A rigid adhesive was therefore used to prevent any curvature of the film and also to get accurate values for the film thickness variations. Such variations are reported in Figure 12 as a function of the applied voltage for 2 samples and a crystal of lithium niobate used here as a reference. Samples A and D of Table III display a quasi-linear amplitude variation only if they have been previously treated by corona discharge. This linear vibration may indicate a piezoelectric behavior of the nanocomposite film provided by the nanorods after their partial orientation. Though quantitative piezoelectric assessments could not be achieved, the linear response of samples A and D is very similar in shape to the one obtained with the $LiNbO_3$ plate. An electrostrictive effect or a Maxwell pressure would indeed result in a second-order response for the vibrations according to the applied AC voltage.

The possible piezoelectric behavior observed in Figure 12 for samples A and D requires optimization before it can be of any practical use and this deserves comments. First, a poor dispersion of $Fe(IO_3)_3$ nanorods and the presence of residual nonpolar aggregates (due to the random orientation of polar nanorods) can prevent any electric-field-induced alignment. In addition, a full dispersion of polar nanoparticles in a fluid matrix may be difficult to preserve. For instance, in the case of ferroelectric $BaTiO_3$ nanoparticles, Evans et al.[42] showed that their aggregation dynamics in nonpolar solvents is related to their dipole moment and that two particles can spontaneously aggregate due to Coulomb attraction with their dipole in opposite direction. As only high electric fields prevent aggregation and even result in disaggregation, we have no evidence that a sufficient high field is reached in our experiment with Corona discharge. It was also assumed here that the polar nature of $Fe(IO_3)_3$ nanorods was not shielded by the matrix and particularly by residual ions of the initial reaction medium. More importantly, in these preliminary experiments, a disruption of the nanoparticle orientation may probably occur during the polymerization step after reorganization of the polymer. Optimal conditions for the poling and photo-polymerization under different cycling temperature, which could not be simultaneously implemented in this study for technical reasons, are thus foreseen.

CONCLUSION

Formation of $Fe(IO_3)_3$ nanorods in microemulsions containing MMA as the oil phase and subsequent photopolymerization were investigated in this study with the aim to prepare transparent piezoelectric nanocomposite films. Incorporation of noncentrosymmetric fillers is clearly attested by the measured optically incoherent SH signal for spin-coated films on glass substrates. Such nanocomposite films could be suitable as in frequency

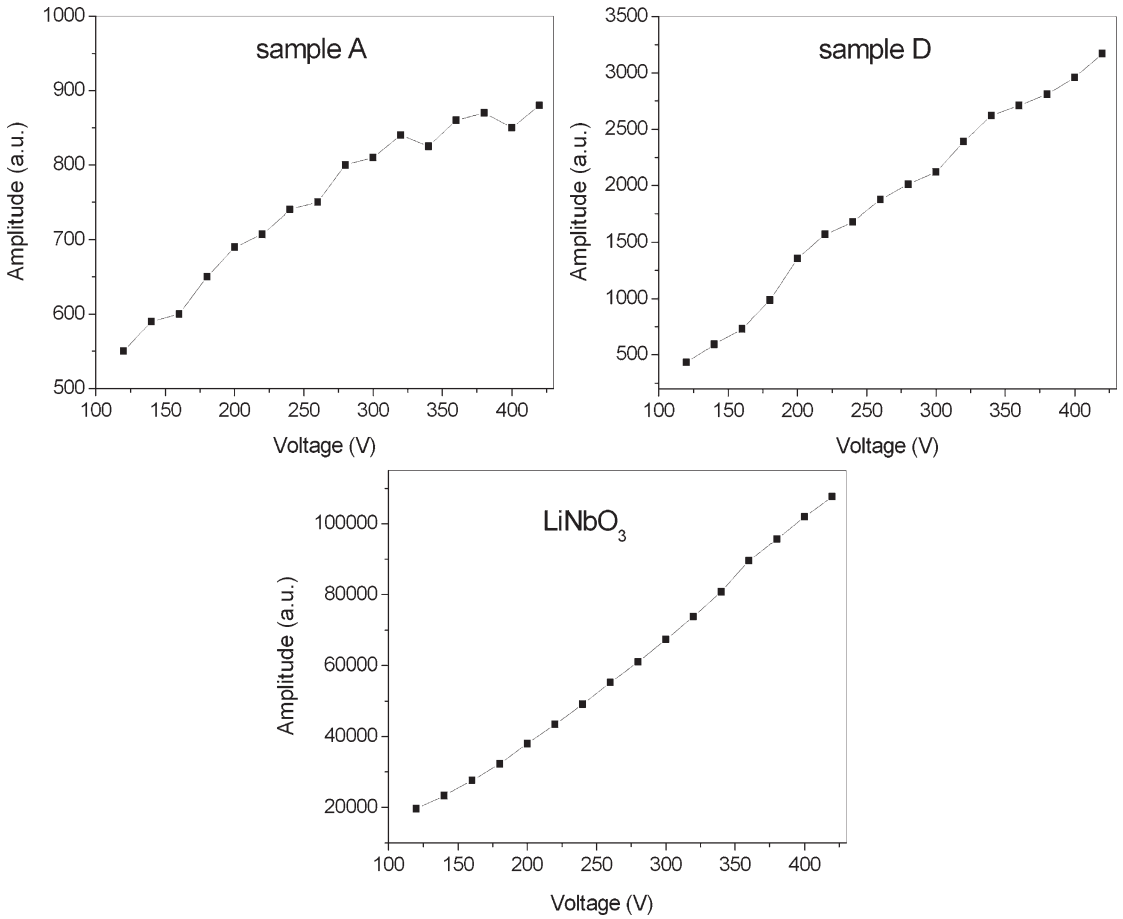

Figure 12. Experimental amplitudes of vibration detected with laser Doppler vibrometry according to the applied voltage for sample A, sample D, and a single crystal of $LiNbO_3$ used as a reference.

conversion devices compatible with standard integration technologies. Development of printable inks with noncentrosymmetric nanofillers could also be relevant in the emerging field of printed electronics if addition of nonlinear optical properties on flexible substrates and smart foils are of interest. In this respect however, full organic polymers obtained after crosslinking of push-pull chromophores are to date more appropriate in terms of material performances, as recently demonstrated.[43]

In the case of organic–inorganic nanocomposites, which are apparently more optically robust, a key issue to address in future works is the achievement of a better control of the nanoparticle orientation within the matrix. Corona discharge treatments applied after deposition of a film and during the crystallization process of iron nanorods were found ineffective for promoting a long-lasting orientation of the growing particles in spite of their crystalline polar structure. A unique, or conversely, a random orientation of the nanofillers can be readily detected by use of the Maker fringes analysis as demonstrated here. Work is thus in progress in order to optimize the experimental conditions to obtain a stable noncentrosymmetry and the corresponding nonlinear optical properties and piezoelectricity. The particularly low cost of polymer matrices indeed deserves special attention for the development of new piezoelectric sensors. In particular, the acoustic impedance of polymer nanocomposites better matches those of liquid and biological media by comparison with bulk materials and makes them attractive for bio-applications.

ACKNOWLEDGMENT

The authors gratefully thank the French *Agence Nationale de la Recherche* (project NANOPOP under grant agreement number ANR-08-NANO-041) and the French competitiveness cluster Plastipolis for financial support as well as Maxence Dermont for his helpful technical support.

REFERENCES

1. Sanchez, C.; Lebeau, B.; Chaput, F.; Boilot, J. *Adv. Mater.* **2003**, *15*, 1969.
2. Sanchez, C.; Julián, B.; Belleville, P.; Popall, M. *J. Mater. Chem.* **2005**, *15*, 3559.
3. Teyssier, J.; Le Dantec, R.; Galez, C.; Mugnier, Y.; Bouillot, J.; Plenet, J. *Appl. Phys. Lett.* **2004**, *85*, 710.
4. Loh, K.; Chang, D. *J. Mater. Sci.* **2011**, *46*, 228.
5. Zhao, Y.; Loh, K.; Chang, D. In Structures Congress 2010, Proceedings of the 19th Analysis & Computation Specialty Conference, Orlando, Florida, May 12–15, 2010, S.

Senapathi, Ed.; American Society of Civil Engineers, **2010**; pp 117–127.

6. Dodds, J.; Meyers, F.; Loh, K. *IEEE Sens. J.* **2011**, *12*, 1889.
7. Mailis, S.; Sones, C.; Scott, J.; Barry, I.; Smith, P.; Eason, R. *Recent Res. Dev. Appl. Phys.* **2004**, *7*, 334.
8. Althues, H.; Henle, J.; Kaskel, S. *Chem. Soc. Rev.* **2007**, *36*, 1454.
9. Althues, H.; Simon, P.; Kaskel, S. *J. Mater. Chem.* **2007**, *17*, 758.
10. Henle, J.; Kaskel, S. *J. Mater. Chem.* **2007**, *17*, 4964.
11. Chai, R.; Lian, H.; Li, C.; Cheng, Z.; Hou, Z.; Huang, S.; Lin, J. *J. Phys. Chem. C* **2009**, *113*, 8070.
12. Chambion, B.; Goujon, L.; Badie, L.; Mugnier, Y.; Barthod, C.; Galez, C.; Wiebel, S.; Venet, C. *Smart Mater. Struct.* **2011**, *20*, 115006.
13. Galez, C.; Mugnier, Y.; Bouillot, J.; Lambert, Y.; Le Dantec, R. *J. Alloys Compd.* **2006**, *416*, 261.
14. Eschbach, J.; Rouxel, D.; Vincent, B.; Mugnier, Y.; Galez, C.; Le Dantec, R.; Bourson, P.; Krüger, J.; Elmazria, O.; Alnot, P. *Mater. Sci. Eng. C* **2007**, *27*, 1260.
15. Phanon, D.; Mosset, A.; Gautier-Luneau, I. *J. Mater. Chem.* **2007**, *17*, 1123.
16. Bonacina, L.; Mugnier, Y.; Courvoisier, F.; Le Dantec, R.; Extermann, J.; Lambert, Y.; Boutou, V.; Galez, C.; Wolf, J. *Appl. Phys. B: Lasers Opt.* **2007**, *87*, 399.
17. Extermann, J.; Bonacina, L.; Courvoisier, F.; Kiselev, D.; Mugnier, Y.; Le Dantec, R.; Galez, C.; Wolf, J. *Opt. Express* **2008**, *16*, 10405.
18. Extermann, J.; Bonacina, L.; Cuna, E.; Kasparian, C.; Mugnier, Y.; Feurer, T.; Wolf, J. *Opt. Express* **2009**, *17*, 15342.
19. Staedler, D.; Magouroux, T.; Hadji, R.; Joulaud, C.; Extermann, J.; Schwung, S.; Passemard, S.; Kasparian, C.; Clarke, G.; Gerrmann, M.; Le Dantec, R.; Mugnier, Y.; Rytz, D.; Ciepielewski, D.; Galez, C.; Gerber-Lemaire, S.; Juillerat-Jeanneret, L.; Bonacina, L.;Wolf, J. *ACS Nano* **2012**, *6*, 2542.
20. Nassau, K.; Shiever, J.; Prescott, B. *J. Solid State Chem.* **1973**, *7*, 186.
21. Mugnier, Y.; Houf, L.; El-Kass, M.; Le Dantec, R.; Hadji, R.; Vincent, B.; Djanta, G.; Badie, L.; Joulaud, C.; Eschbach, J.; Rouxel, D.; Galez, C. *J. Phys. Chem. C* **2011**, *115*, 23.
22. Nguyen, V.; Rouxel, D.; Hadji, R.; Vincent, B.; Fort, Y. *Ultrason. Sonochem.* **2011**, *18*, 382.
23. Palkovits, R.; Althues, H.; Rumplecker, A.; Tesche, B.; Dreier, A.; Holle, U.; Fink, G.; Cheng, C.; Shantz, D.; Kaskel, S. *Langmuir* **2005**, *21*, 6048.
24. Rouxel, D.; Eschbach, J.; Vincent, B.; Kouitat, R. *Int. J. Surf. Sci. Eng.* **2010**, *4*, 322.
25. Liu, P.; Su, Z. *J. Macromol. Sc. Part B: Phys.* **2006**, *45*, 131.
26. Sun, D.; Miyatake, N.; Sue, H. *Nanotechnology* **2007**, DOI:10.1088/0957–4484/18/21/215606.
27. Galceran, M.; Pujol, M.; Carvajal, J.; Tkaczyk, S.; Kityk, I.; Dáz, F.; Aguiló, M.; *Nanotechnology* **2009**, DOI:10.1088/0957–4484/20/3/035705.
28. Macchi, R.; Cariati, E.; Marinotto, D.; Roberto, D.; Tordin, E.; Ugo, R.;Bozio, R.; Cozzuol, M.; Pedron, D.; Mattei, G. *J. Mater. Chem.* **2010**, *20*, 1885.
29. Liu, H.; Ye, H.; Zhang, Y.; Tang, X. *Dyes Pigm.* **2008**, *79*, 236.
30. Lin, D.-J.; Don, T.-M.; Chen, C.-C.; Lin, B.-Y.; Lee, C.-K.; Cheng, L.-P. *J. Appl. Polym. Sci.* **2008**, *107*, 1179.
31. Althues, H. Lumineszierende, transparente Nanokomposite-Synthese und Charakterisierung. Ph.D. Thesis,Technischen Universität Dresden, 2007.
32. Ladj, R.; El-Kass, M.; Mugnier, Y.; Le Dantec, R.; Fessi, M.; Galez, C.; Elaissari, H. *Cryst. Growth Des.* **2012**, *12*, 5387.
33. Cölfen, H.; Mann, S. *Angew. Chem. Int. Ed.* **2003**, *42*, 2350.
34. Delahaye, E.; Tancrez, N.; Yi, T.; Ledoux, I.; Zyss, J.; Brasselet, S.; Clément, R. *Chem. Phys. Lett.* **2006**, *429*, 533.
35. Delahaye, E.; Sandeau, N.; Tao, Y.; Brasselet, S.; Clément, R. *J. Phys. Chem. C* **2009**, *113*, 9092.
36. Vincent, B.; Krüger, J.; Elmazria, O.; Bouvot, L.; Mainka, J.; Sanctuary, R.; Rouxel, D.; Alnot, P. *J. Phys. D: Appl. Phys.* **2005**, DOI:10.1088/0022–3727/38/12/026.
37. Bactavatchalou, R.; Alnot, P.; Bailer, J.; Kolle, M.; Müller, U.; Philipp, M.; Possart, W.; Rouxel, D.; Sanctuary, R.; Tschöpe, A. *J. Phys.: Conf. Ser.* **2006**, DOI:10.1088/1742–6596/40/1/014.
38. Hadji, R.; Nguyen, V.; Vincent, B.; Rouxel, D.; Bauer, F. *IEEE Trans. Ultrason. Eng.* **2012**, *59*, 163.
39. Vigolo, B.; Vincent, B.; Eschbach, J.; Bourson, P.; Maréché, J.; McRae, E.; Müller, A.; Soldatov, A.; Hiver, J.; Dahoun, A. *J. Phys. Chem. C* **2009**, *113*, 17648.
40. Q. Zhang, W. Pan, L. Cross, *J. Appl. Phys.* **1988**, *63*, 2492–2496.
41. Herdier, R.; Jenkins, D.; Dogheche, E.; Rèmiens, D.; Sulc, M. *Rev. Sci. Instrum.* **2006**, *77*, 093905.
42. Evans, D.; Basun, S.; Cook, G.; Pinkevych, I.; Reshetnyak, V. *Phys. Rev. B* **2011**, *84*, 174111.
43. Centore, R.; Borbone, F.; Fusco, S.; Carella, A.; Roviello, A.; Stracci, G.; Gianvito, A. *J. Polym. Sci. Part B: Polym. Phys.* **2012**, *50*, 650.